*Manuscript
Click here to view linked References

Wind-induced natural ventilation of re-entrant bays in a high-rise building

Cheng C.K.C. Department of building and construction, City university of Hong Kong, Hong Kong (bcccheng@cityu.edu.hk)

Lam K.M. Department of Civil Engineering, University of Hong Kong, Hong Kong (kmlam@hkucc.hku.hk)

Leung Y.T.A Department of Building and Construction, City University of Hong Kong, Hong Kong SAR (bcaleung@cityu.edu.hk)

Yang K. Laboratory of Tibetan Environment Changes and Land Surface Processes, Institute of Tibetan Plateau Research, Chinese Academy of Sciences, Beijing, PRC (YangK@itpcas.ac.cn)

Danny H.W. Li Department of building and construction, City university of Hong Kong, Hong Kong (bcdanny@cityu.edu.hk)

Sherman C.P. Cheung School of Aerospace, Mechanical & Manufacturing Engineering, RMIT University, Australia (chipok.cheung@rmit.edu.au)

Corresponding Author: CHENG Chor Kwan, Charles

Postage address: Department of Building and Construction, City University of Hong Kong, 83 Tat Chee Avenue, Kowloon, Hong Kong

Telephone: (852) 2788 7618

Fax: (852) 2788 9446

email: bcccheng@cityu.edu.hk

ABSTRACT

This paper reports a systematic computational study of wind-induced natural ventilation and pollutant transport of re-entrant bays on a total of 30 generic building models of different building heights and with bays of different dimensions. Mean wind flow around each building model and wind-induced flow inside re-entrant bays are computed. To determine the ventilation efficiency of the bay, the computed flow field is used to disperse a scalar pollutant initially occupying the entire bay at a uniform concentration. The subsequent time decay of pollutant concentration inside the bay is studied and the ventilation efficiency is quantified by the retention time. The results show that wind-induced flow inside the bay, especially on the building side face, is complex and highly three-dimensional. Air exchange rates through the roof opening and vertical side opening are analyzed for each bay and their relationship to the ventilation efficiency is discussed. The bays on the building side faces are much worse ventilated than those on the windward or leeward building face. The deeper the side bay, the worse is the air exchange and ventilation. The building height is found to have a governing effect on the ventilation of the windward and leeward re-entrant bays.

Keywords: Natural ventilation, High-rise building, Wind-Structure Interaction, Micro-climate, CFD simulations, Re-entrant bays, Pollutant dispersion

1. Introduction

Wind effects play an important role in building ventilation. Wind breezes are always desirable for cooling in warm weathers and for wind-induced dispersion of unwanted emissions from a building. For a low-rise house, wind can often be collected by large scale wide open features, like atriums or courtyards (Aldawoud and Clark, 2008; Rajapaksha et al., 2003; Sharples and Bensalem, 2001). But these architectural features are not easily adopted by high-rise buildings. For high-rise multi-apartment residential buildings, which are increasing common in metropolitan cities, it is important to optimise between views and ventilation. In order to satisfy both requirements, these high-rise buildings often adopt an irregular cross-sectional shape with apartments arranged as wing sections extending from a central core. Between adjacent building wings are deeply-recessed re-entrant bays (recessed cavities) or "light-wells" towards which kitchen and bathrooms windows open. Unwanted matters and heat are emitted into the re-entrant bays which do not occupy the most important views of the building. It is essential that these emissions can be dispersed out of the re-entrant spaces effectively by wind-induced natural ventilation.

The measurement results of Higson et al. (1996) showed that wind-driven pollutant dispersion around a building was dependent on the building shapes. Gomes et al. (2005) and Santos et al. (2005) also found that wind flow around a building behaves interactively with the basic geometry of the building. Installation of a re-entrant bay in a building is expected to lead to a particular pattern of wind flow around the building and inside the bay, which in turn determines wind-induced ventilation characteristics of the re-entrant bay.

While there have been many studies investigating wind loads acting on different shaped buildings (Kijewski and Kareem, 1998; Zhou et al., 2003), very few studies provide the essential details of wind flow information inside a building re-entrant bay. The wind loading study of Building Research Establishment (Cook, 1985) suggested that wind flowing around a building with recessed corners or re-entrant bays intends to skip past a narrow recessed bay and leave an almost stagnant flow inside it but details of flow information were not provided. Chow et al. (2002) carried out a computational fluid dynamics (CFD) study of wind flow around a building with a re-entrant bay installed at the mid-width of the building front face. They pointed out that at this normal incidence, some flow might come down the re-entrant bay from its roof opening face if there was no heat discharged into the bay.

In real-life situations, a poorly ventilated re-entrant bay can lead to disastrous consequences in the built environment. In 2003, Hong Kong experiences the outbreak of Severe Acute Respiratory Syndrome (SARS) Crises with almost 300 people died (Yeoh, 2003). Many victims lived in Amoy Garden, a group of high-rise multi-apartment buildings. The first patient lived on the 16^{th} floor of a 36-storey residential building. The level was about 1/3 times the building height (H) above its podium. After a very short period, there were more than 200 cases found in the same housing but there were no cases reported at a level below 9^{th} floor ($0.15H$). A subsequent study by building and medical professionals in Hong Kong suggested that the SARS virus might be discharged from the bathroom of the infected unit and subsequently spread to the other rooms through air flow paths inside the re-entrant bay (Hong Kong Government, 2004). The re-entrant bays of Amoy Garden buildings are deeply recessed into the building side walls, having a width-to-depth (W/D)

ratio of 0.25~0.33. According to Cook (1985), flow inside these deep recessed bays is largely stagnated. And this stagnant flow condition would prolong a long-time residence of SARS viruses emitted into the bay and thus increasing the chance of their transmission into the connecting apartments through air exchange with the bay (Yu et al., 2004). This event demonstrates the importance of wind-induced natural ventilation of re-entrant bays in buildings for dispersion of pollutants and matters. Other adverse consequences of poor natural ventilation of the re-entrant bays include increased risks of environmental health and fire safety of the building that may arise from poor dispersion of waste gases or fire smoke discharged into the bay. In warm regions, domestic air conditioners often have their air-cooled condensers installed inside the re-entrant bays and insufficient ventilation of the bays may lead to increase in energy consumption as a result of built up of condensing temperature.

The present paper aims at a systematic investigation of wind-induced flow inside and around generic re-entrant bays of a tall building and the associated ventilation efficiency with CFD simulations. The generic building models aim to represent common full-scale tall residential buildings in a metropolitan city such as Hong Kong. The CFD technique has been successfully applied by the authors to study wind-induced natural ventilation of a refuge floor which is also a large recessed feature of the tall buildings (Cheng et al., 2005; Cheng et al., 2007; Cheng et al. 2008; Cheng, 2009).

2. Test cases of tall buildings and re-entrant bays

The objectives of this study are to determine the wind-induced ventilation flow inside a generic re-entrant bay of varying dimension, and to determine its effects on pollutant dispersion out the bays.

A tall building with a cross section of an "**H**" shape is chosen as the generic building configuration. Two re-entrant bays are thus presented on two opposite walls of the building. The "**H**" shaped cross section has a square envelope of breadth *B.* Nine "**H**" shapes are studied and their configurations were listed in Table 1. In these "**H**" shapes, the horizontal dimensions of the re-entrant bay vary in a systematic manner which covered three different widths; $W/B = \{0.25, 0.5, 0.75\}$, and three different depths; $D/B = \{0.125, 0.25, 0.375\}$. Flow over a square building with no re-entrant bay is also studied. Three groups of buildings with different building height; $H/B = \{4, 6, 8\}$, are studied. Including the control square buildings, wind flow over a total number of 30 buildings are computed in this study. In addition, computations are carried out for each building at two wind incidence angles. At wind angle 0^o, wind blows normally onto the building face with a re-entrant bay (Table 1). At wind angle 90^o, the re-entrant bays are on the two side faces of the building.

The breadth of the building is targeted at full-scale value of $B = 30$ m. The building heights being studied thus vary between 120 m and 240 m. These building dimensions are typical of high-rise residential buildings in Hong Kong.

3. CFD simulations

The same CFD technique used by the authors to study wind flow problems around a tall buildings (Cheng et al., 2005; Cheng et al., 2007; Cheng et al. 2008; Cheng, 2009) is applied in the present study. Three-dimensional (3D) flow simulations are carried out by ANSYS CFX at a reduced geometric scale of 1:300, which is also the scale of the accompanying wind tunnel tests. The computational domain has a width at 3 m and a height at 1.7 m. These values match the cross-sectional dimensions of the boundary layer wind tunnel of the Department of Civil Engineering at the University of Hong Kong where some flow measurements around models of **H**-shaped tall buildings are carried out. The computational domain has a length of 6 m and the building model is located at 1 m downstream of the inlet plane of the domain. This means that there will be more than 1*H* distance upstream the building and at least 6*H* downstream distance between the building and the inlet or outlet plane. The 3D computational domain is discretized into unstructured tetrahedral elements with element sizes stretching progressively outwards from the building walls to the domain boundary walls (Fig. 1). In regions far from the building, no element has a dimension greater than 0.1 m and mesh elements generated close to the building walls are refined to have a minimum dimension of 0.01 m so as to fulfil the application requirements of the wall functions. The numbers of computation elements range from 4 to 8 Millions and this mesh resolution complies with the recommended requirements of AIJ (Tominaga et al., 2008) for computational wind flow studies of buildings.

The CFD computation seeks a steady solution of the 3D turbulent flow with the RANS (Reynolds Averaged Navier Stokes) method. Turbulence closure is made with the standard k-ε model (Launder and Spalding, 1974). This model applies gradient diffusion hypothesis to relate Reynolds stresses to mean velocity gradients and turbulent viscosity.

Turbulent viscosity is modelled as the product of turbulent velocity and turbulent length scale. While the turbulence velocity scale is calculated by solving the transportation equation for turbulent kinetic energy (k), the turbulent length scale is estimated by solving the transportation equations for the k and its dissipation rate (ε). The governing equations (Ansys CFX-solver theory guide, 2009) for the simulations are listed as follows:

- Continuity Equation

$$\frac{\partial \rho}{\partial t} + \nabla \cdot (\rho \boldsymbol{U}) = 0 \qquad (1)$$

- Momentum Transportation Equation

$$\frac{\partial \rho U}{\partial t} + \nabla \cdot (\rho U \otimes U) - \nabla \cdot (\mu_{eff} \nabla U) = -\nabla p' + (\nabla \mu_{eff} \nabla U)^Y + B \qquad (2)$$

where $p' = p + \frac{2}{3}\rho k$; $\mu_{eff} = \mu + \mu_t$ and $\mu_t = C_\mu \rho \frac{k^2}{\varepsilon}$

- Transportation Equation for k

$$\frac{\partial (\rho k)}{\partial t} + \nabla \cdot (\rho \boldsymbol{U} k) = \nabla \cdot \left[\left(\mu + \frac{\mu_t}{\sigma_k} \right) \nabla k \right] + P_k - \rho \varepsilon \qquad (3)$$

- Transportation Equation for ε

$$\frac{\partial (\rho \varepsilon)}{\partial t} + \nabla \cdot (\rho \boldsymbol{U} \varepsilon) = \nabla \cdot \left[\left(\mu + \frac{\mu_t}{\sigma_\varepsilon} \right) \nabla \varepsilon \right] + \frac{\varepsilon}{k} (C_{\varepsilon 1} P_k - C_{\varepsilon 2} \rho \varepsilon) \qquad (4)$$

- Model Constants

$C_{\varepsilon 1}$ = 1.44, $C_{\varepsilon 1}$ = 1.92, C_{μ} = 0.09, σ_k = 1.0, and σ_{ε} = 1.3

Characteristics of natural wind are set as the inflow boundary conditions at the inlet of the computational domain. Power-law wind profiles typical of an open land exposure (Lam and To, 2006; Lam et al., 2008) are used for of mean wind velocity, $U(z)$, and turbulence intensity, $I(z)$:

$$\frac{u}{U_{ref}} = \left(\frac{z}{z_{ref}} \right)^{0.19} \tag{5}$$

$$\frac{I}{I_{ref}} = \left(\frac{z}{z_{ref}} \right)^{-0.47} \tag{6}$$

where U_{ref} = 10.48 m/s, I_{ref} = 0.088 and z_{ref} = 0.85 m. The other two mean wind velocity components v and w are set to be zero. At the outlet, the relative static pressure is taken to be zero and Eq. (6) is applied again.

The authors have investigated wind flow patterns around a number of tall building configurations using this RANS-based CFD approach (Cheng et al., 2005; Cheng et al., 2007; Cheng et al. 2008; Cheng, 2009; Lam and To, 2006; Lam et al. 2008) in which details of model set up and validation have been presented. For the study of wind-induced flow through a refugee floor on an intermediate level of a tall building, the computed flow vectors have been compared to measured velocities in a wind tunnel model (Cheng et al., 2005) and the mean velocity components u/U_H are repeated there in Fig. 2. In the computation of pedestrian-level wind around a group of tall buildings (Lam and To, 2006), extensive comparison has been made between computed and wind tunnel flow vectors. In

the present study, some wind flow velocities around an **H**-shaped tall building model are measured in the wind tunnel with a 7-hole cobra probe (Aeroprobe, Inc.) on the horizontal plane at mid-building height. The probe can measure 3D velocity components for flow coming within a cone of 70^o from its axis. In the measurement, the probe is aligned towards the approaching wind direction and reliable data are obtained in regions around the building. Fig. 3 shows a comparison of the computed and measured flow vectors for the 0.6 m tall building model with Case 2 re-entrant bays. The measured flow vectors show the separated wind flow from the building upwind corner. Accurate numerical reproduction of this separated flow is a challenge for RANS-based CFD. Imposing the measured turbulence intensity profile as a boundary condition is essential. It is observed in Fig. 3 that the computed flow vectors tend to over-predict slightly the size of the separation region but there is reasonable agreement between wind tunnel data and CFD results. The present wind flow simulations are performed on a 64-bit quad-core computer and it takes about 6 hours to complete one simulation. In terms of numerical accuracy, iterations are stopped when the average root-mean-square residual of the final iteration step is reduced to below 0.000001.

Subsequent to the computation of wind flow patterns, the second part of the study is concerned with the dispersion of matter and pollutants inside the re-entrant bay. For this purpose, wind-induced ventilation of the re-entrant bay filled initially with a passive scalar is studied. This enables the wind-induced flushing behaviour of the bay or the retention time of the scalar pollutant inside the bay to be studied and compared among re-entrant bays of different dimensions. In the computation, a passive and non-buoyant scalar species is used to represent a pollutant and this scalar species is set to fill up the entire volume of

the re-entrant bay under study at a uniform concentration at time zero. Afterwards, the scalar is dispersed by the computed wind flow field.

Simulation of the dispersion of pollutant from the re-entrant bay is carried out at non-uniform time steps lasting from time 0 to 1.5 s. After 1.5 s (model scale), nearly all scalar is found to be removed from the re-entrant bay in most cases. The mean dispersion or dilution level of the scalar pollutant inside the re-entrant bay at different times is described by a residual concentration coefficient. This is calculated by a normalisation of the volume-average mean scalar quantity (C) occupying the re-entrant bay volume at each time step by its initial uniform value (C_o) at the beginning of a simulation. The ventilation efficiency can be compared via the retention time (Yim 2009) which is the time when the residual concentration coefficient drops to the value of $1/e$ (≈ 0.368).

This part of dispersion is also carried out at the same two wind angles of 0^o and 90^o for the 30 different buildings. This provides information on the ventilation efficiency of three types of re-entrant bays. They are a re-entrant bay on the windward face of the building under normal wind incidence onto it, a re-entrant on the leeward face, and a re-entrant bay on the side face (at wind angle 90^o). These simulations are carried by a 64-bit SGI HPC computer server and 24 CPUs are deployed. A computational time of about 1 hour is required to produce the results of pollutant dispersion for 1.5 s (model scale). The iteration threshold for these simulations is lower to the acceptable limit of 0.0001 for the average root-mean-square residual.

4. Wind-induced flow patterns and air exchange rate

The first part of CFD computation gives the solutions of the mean velocities and mean pressure in the flow field, as well as other statistical turbulence properties such as the turbulence kinetic energy and dissipation rate. The flow patterns are provided by the 3D velocity components, *u*, *v*, and *w*, in the *x* (along-wind), *y* (transverse), and *z* (vertical) directions. Their magnitudes depend, of course, on the prevailing wind speed. Thus, the velocities are normalized by U_H, the unobstructed wind speed at the building height level. Similarly, wind pressure is presented as pressure coefficient (C_p):

$$C_p = \frac{p - p_H}{\frac{1}{2}\rho\left(U_H\right)^2} \tag{7}$$

where P_H is the reference pressure taken on the inlet flow plane at the building height level. In this study, two areas of focus are placed on the computed wind flow field. The first is the wind flow around the building as a whole and the question is whether presence of the re-entrant bays leads to any significant modification to this flow pattern. In general, we observed from the computational results at wind angles 0^o and 90^o that the main wind flow structures forming around the buildings are not being altered significantly by the presence of two re-entrant bays at the building two opposite sides. A sample comparison is shown in Fig. 4 demonstrate this general observation.

Our second focus is the patterns of wind-induced flow inside a re-entrant bay. The flow patterns are found to be highly 3D and complicated and to simplify the discussion, some measures of air exchange rate or ventilation efficiency are used. The flow going into or leaving the bays occurs either through the open (vertical) face of the bay or the top opening (horizontal). The flowrate through the vertical bay face varies with height and can

be inward (negative) or outward (positive). A local normal velocity coefficient is defined to quantify this flow exchange rate between the bay and the outside through the vertical bay opening:

$$C_n(z) = \frac{1}{U_H \cdot W \cdot \Delta z} \int_{-W/2}^{+W/2} \int_{z}^{z+\Delta z} u_{normal}\, dn\, dz \tag{8}$$

where $dn = dx$ for a windward or leeward re-entrant bay whereas $dn = dy$ for a side bay. The integration of the velocity component normal to the vertical bay opening face, u_{normal}, is carried out along a local vertical section of the opening. For the re-entrant bay on the windward or leeward building face (at wind angle 0^o), u_{normal} is the u velocity component in the computational coordinates. For the re-entrant bay on the building side face building (at wind angle 90^o), it is the v velocity component. The coefficient is actually the mean normal velocity averaged along that section of the opening and normalized by the mean wind speed at building height. On the other hand, the local average vertical flow inside the bay is represented by a local vertical velocity coefficient defined as:

$$C_w(z) = \frac{1}{U_H \cdot D \cdot W} \int_{-W/2}^{+W/2} \int_{-D/2}^{+D/2} w\, dx\, dy \tag{9}$$

The value of C_w at $z = H$ represents the rate of air flow leaving the bay through its roof opening. By continuity, the difference in lateral air exchange rate $C_n(z)$ between two successive levels must be balanced by a net vertical upward or downward flow $C_w(z)$ inside the bay. Thus, in some of the results, only the vertical distributions of $C_n(z)$ are presented and the distributions of $C_w(z)$ are not shown by the values except the values at the roof opening.

4.1. Wind-induced natural ventilation of re-entrant bay at wind angle 0^o

At wind angle 0^o, wind blows normally onto the building face with a windward re-entrant bay. The bay is expected to be under active wind-induced ventilation. On the other hand, the bay on the leeward building face is in the wake of the building and its ventilation relies on flow induced by the pressure distribution around it.

Fig. 5 shows the results of the selected case of a building of $H/B = 6$ with Case 5 bays; i.e. $W/B = 0.5$ and $D/B = 0.25$. Horizontal flow vectors of (u, v) are shown at the mid-height level and the general observation is that although wind blows onto the windward building face, little flow enters the re-entrant bay. Wind speeds inside the windward bays often have small magnitudes as compared with the incident wind speed and wind speeds are found to be even slower in a taller building. For the control square tall building, our computation results have shown low-speed reversed flow approaching the leeward building face on the mid-height plane (Fig 4). The same global flow behavior is observed on the leeward face of the **H**-shaped buildings. Similar to the windward face, only little flow enters into the leeward side re-entrant bays. Another general observation from all the computation results is that the amount of flow going into the re-entrant bays seems related to the width of the bays while the depth has a minor influence. More flow can enter the wider bays, both on the windward and leeward building faces.

The computed pressure distribution in Fig. 5 shows that the back face of the windward bay is under the stagnation effect in a similar manner as on the windward face of a building without a bay. At $z \approx 0.8H$ to $0.85H$, there is a time-average mean stagnation point on the back face of the bay. A high positive pressure at $C_p > 0.9$ is found around the stagnation point. Above this height, wind flows into the bay with upward w components to

escape through the roof opening. At levels below the height of the stagnation point, wind flows with downward *w* components into the bay, except at levels near the ground where air flows out of the bay. Thus, C_p decreases in magnitude towards the ground. At levels near the ground, the downward flow hits the ground slab and curves outwards to leave the bay, leading to a recovery of pressure around the building base level. Inside the lower half of a deep re-entrant bay, the downward *w* components become very much greater than the along-wind *u* components and the flow is primarily wholly in the downward direction.

On the leeward side, the pressure coefficients in Fig. 5 are rather uniform at $C_p \approx -0.4$ which is a typical situation in the wake behind a building. The flow around the rear bay occurs mainly in the reverse direction and with slow speeds. In most cases, the variation of flow patterns with height is the reverse of that on the windward side but with much lower speeds. One difference is that the stagnation point of the reverse flow occurs at a lower height at $z \approx 0.6H$. Another difference is that the flow leaves the roof opening with almost vertical directions.

In terms of wind-induced ventilation, the integral rate of flow exchange between the bay and the outside space is more relevant. Figs. 6(a-b) show the vertical distributions of $C_n(z)$ for, respectively, the windward and leeward re-entrant bays of width $W/B = 0.5$. The distributions for bays of the other two width values are similar and not shown for brevity. The distributions of $C_w(z)$ are not shown but the values at the roof opening are presented in Fig. 6(c).

Fig. 6 shows that little air exchange occurs on the middle building levels between the windward bays and their outside. Only at and above the stagnation point level that wind causes significant amount of flow to enter the bay. This inflow rate increases towards the

building top level. One part of this amount of air entering the bay goes up and leaves the bay through the roof opening. The other part travels down the bay with little net air exchange with the outside and leaves the bay at levels near the ground, $z/H < 0.2$. The distributions are similar for bays of different widths or depths, bay or different building heights. The magnitudes of the normal outflow velocity coefficient near the building top or bottom levels are, however, dependent on those dimensions. A larger peak C_n is found in deeper bays while the width of the bay has no noticeable effect. The shorter buildings, $H/B = 4$, have slightly larger values of peak C_n but this occur over a shorter physical vertical distance (over similar ranges of z/H but H is physically smaller) so that the absolute amount of air inflow rate is not as high as that on a taller building. As a result, the amount of air leaving rate through the roof opening, as measured by $C_w(H)$, increases with the building height (Fig. 6(c)). The dependence of $C_w(H)$ on the bay dimensions is that a higher average vertical velocity occurs at the roof opening of a narrower and shallower bay. The dependence, as shown in Fig. 6(c), is only at a slight degree and the absolute amount of air flow rate (which is caused by $C_w(H)$ and the bay cross-sectional area) still increases with the size of the bay.

For the leeward bay, air flow is passively induced. There is a much weaker stagnation region and at a lower heights than that on the windward side. Thus, air is induced to enter the bay through almost the entire upper part of the building heights. Only at $z/H < 0.2$ that air flows out of the bay near the ground (Fig. 6(b)). Compared with the actively ventilated windward bay, a much smaller rate of air outflow occurs through the roof opening of the leeward bay. Another difference in Fig. 6(c) is that $C_w(H)$ at the rear face

decreases with the building height and increases with D/B. This may be because the passively induced flow is heavily affected by the flow resistance through the bay.

4.2. Wind-induced natural ventilation of side re-entrant bays

At wind angle 90^o, the two re-entrant bays are on the side faces of the building and fully immersed in the separation wake. Flow inside the bay is induced by the external wind flow and there is no active ventilation of the bay. Our computed results show that the flow inside the bay is highly 3D and exhibit complex patterns with strong dependence on the bay dimensions and building height. Fig. 7 shows, as an example, the mean flow patterns inside the re-entrant bay of size $W/B = 0.75$, $D/B = 0.375$ on a building of $H = 8B$. Flow vectors on three horizontal planes at different heights are shown in Fig. 7(a), and the computed flow vectors of (v, w) on the vertical y-z plane at $x = 0$, that is the mid-width plane of the bays; are shown in Fig. 7(b). Results for other buildings are not shown but the general observation is described.

At the two upper heights in Fig. 7(a), low-speed recirculating flow on the horizontal plane is found inside the re-entrant bay. Inside a shallow and wide bay of $D = 0.125B$ and $W > 0.25B$, this circulation vortex structure is poorly developed and occupies a small region close to the leeward wall of the bay. When a bay has an aspect ratio (W/D) near unity, the entire cross section of the bay is occupied by a well-developed circulation vortex. This well-developed vortex flow is observed on the taller buildings at $H/B = 6$ and 8 but not on the shorter buildings. This may be due to a change in vertical location of the vortex structure. At the lower height, the mean flow vectors in Fig. 7(a) do not show the pattern of

a circulation vortex. This is generally observed at heights where there is significant fluid circulation on the vertical plane (Fig. 7(b)).

The flow vectors on the vertical plane in Fig. 7(b) show complex secondary flow structures inside the re-entrant bay. These structures have fluid circulation on the *y*-*z* plane; that is streamwise *x*-vorticity. The most obvious of these large-scale vortical structures is found near the ground, at $z/H < 0.3$ in Fig. 7(b). This vortex is observed inside almost all re-entrant bays under study and is particularly well-developed in deeper bays and in taller buildings. Fluid circulation of this vortex brings in air from outside the bay near the ground and ejects air out of the bay at a higher level, at $z/H \approx 0.3$ in Fig. 7(b). Presence of this vortex blocks the downward flow stream from reaching the ground.

In terms of pressure distribution, the region next to the building side walls and inside the bay (at this plane of $x = 0$) is under quite uniform wake pressure around $C_p \approx -0.45$. Pressure at similar values is also found near above the building roof. On the building mid-height level, the pressure is slightly more negative and this causes flow to enter the re-entrant bay, at z/H between 0.4 and 0.8 in Fig. 7(b). A stream of this flow goes down the bay and joins itself into the fluid circulation of the large secondary flow structure near the ground. Another stream of the entering flow goes up inside the bay and towards the roof opening. For a shallow re-entrant bay, this flow escapes through the roof opening, leading to the "chimney effect". For a deeper bay such as the one in Fig. 7(b), however, escaping roof through the roof opening occurs in the outer part of the opening and some escaped flow is entrained back into the bay through the inner part of the opening. This leads to another secondary-flow vortical structure with well-developed *x*-vorticity located near the roof opening.

The vertical velocity coefficients at the roof, $C_w(H)$, are shown in Fig. 8(a). It is evident that the "chimney effect" flow out of the bay roof opening occurs only for the shallower bays at $D = 0.125B$. The distributions of vertical air transport inside the side re-entrant bays are shown by $C_w(z)$ in Fig. 8(b), for buildings of height $H = 6B$. It is clear that flow inside the mid-height portion of the bays is in the downward direction. The vertical distribution of air exchange between the bay and the wake region outside the building side face is shown by the profiles of $C_n(z)$ shown in Fig. 9. They are for a re-entrant bay on the $-y$ side face of the building so that positive values of $C_n(z)$ mean a net flow of air into the bay at that height. In general, the air exchange pattern along the building height is consistent with the flow patterns described. The secondary-flow vortex at the base of the bay brings in air near the ground and ejects air at some distances above ground. For the taller buildings, this air exchange occurs below $z/H < 0.2$ to 0.3 and at the building mid-height levels, slow rate of air flows into the bay. However, for the shorter buildings ($H/B = 4$), the ground vortex occupies a large size and reaching the building mid-height so that air flows out of the bay on all middle levels. Near the building roof level, $z \geq 0.8H$, air is always drawn into the bay by the vortex near the roof opening.

5. Pollutant dispersion from the re-entrant bays

The ventilation efficiency of the re-entrant bays is investigated in the second part of the computation. At wind angle 0^o, pollutant initial filling the windward side re-entrant is dispersed by active wind flow. Following the distribution of $C_n(z)$ in Fig. 6, pollutant will

be dispersed out of the re-entrant bay from and near the roof opening face and near the base of the vertical opening face. This transport path is clearly illustrated in Fig. 10(a) which shows the pollutant residual concentration coefficient, C/C_o, on the vertical symmetry plane of re-entrant bay having dimensions W/B = 0.25 and D/B =0.375 on a tall building of H = 8B at successive time instants. It can observed that while the flow through the roof opening disperses the pollutant from the upper part of the bay quite quickly, the outflow near the base of the bay is slower in removing the pollutant from the middle and lower part of the bay. Furthermore, the expelled pollutant is brought along the ground upwind for a longer distance to form a thin level of low concentration pollutants. The inner base corner of the re-entrant bay takes the longest time to clear out the pollutant concentration.

The dispersion of pollutant out of the re-entrant bays of different configurations on the windward face of the buildings, and also on other faces, exhibit similar pattern of C/C_o decay with time. The decay rate is rapid at the beginning but starts slowing down after the concentration level drops to $C/C_o < 0.1$. As an illustration, Fig. 11 shows these decay curves for the re-entrant bays of W/B = 0.25. It can be observed that for the deeper bays, the decay is slower for the bays in a taller building. Little differences are observed for the shallowest re-entrant bays with D/B = 0.125.

Fig. 12(a) compares the ventilation efficiencies of the 27 different re-entrant bays using the retention times. It is obvious that a taller height of the building or the re-entrant bay always leads to a longer retention time, which means poorer ventilation or slower dispersion of pollutant. This is because the transport paths are mainly from the roof opening and from near the ground (Fig. 10) so that it takes a longer time to ventilate a taller bay. Fig. 12 clearly shows that the narrowest bays (at W/B = 0.25) are the worst ventilated and the

widest bays (at $W/B = 0.75$) have the shortest retention times. For the widest bays, the retention time increases with the bay depth (D/B) in a near-proportional manner.

As described earlier, the air exchange paths of the re-entrant bay on the leeward face of the building are similar to those on the windward bay. This results in similar dispersion behaviour of the leeward bay as shown in Fig. 10(b) where pollutant leaves the bay from the horizontal roof opening face and from the vertical opening face near the ground. The pollutant leaving the roof opening is brought slightly upwind over the building roof before being blown downward by the separation flow from the building roof. The pollutant leaving the bay near the ground surface keeps flowing along the ground up to about $2.5B$ distance behind the building rear face before it is lifted upward and slightly upwards, probably due to the recirculation flow behind the building as a whole (Lam and To, 2006).

Similar decay rates of pollutant concentration inside the bays are found for the leeward bays as those in Fig. 11 but the rates of decay are much slower. Fig. 2(b) compares the retention times of the 27 re-entrant bays on the leeward face of a tall building. The values of retention times are longer than those of the windward bays by a factor of about 1.5. Since the air exchange paths are similar to the case of the windward bays, that is, from the roof and the base of the bays, the retention time is found to increase with H. Similar effects of the bay widths and depths on the retention time are observed as for the windward bays.

Re-entrant bays on the building side face are passively ventilated and the dispersion of pollutant out of these bays takes a much longer time than the windward or leeward bays. Fig. 13(a) shows the progress of dispersion of a deep re-entrant bay of dimensions $W/B = 0.25$ and $D/B = 0.375$ on a $H = 8B$ tall building. As described earlier, air exchange is

dominated by the large secondary-flow vortex near the ground level which brings in clear air from outside and ejects pollutant-laden air at a short height above. This effect on pollutant dispersion is clearly observed in Fig. 13(a). For this deep bay, the roof vortex mainly acts to bring in clear air from outside and thus diluting the pollutant concentration near the top of the bay. Fig. 8 has shown that the flow is mainly vertically downward inside the deep bays. This explains why the pollutant cloud in Fig. 13(a) is retracting towards its lower edge and why there is little dispersion out from the vertical opening of the bay.

Fig. 13(b) shows the dispersion of a shallow bay at $D/B = 0.125$ and it is evident that it is much better ventilated than the deep bay in Fig. 13(a). This is because the small flow out of the vertical opening of the bay is sufficient to disperse a larger portion of the pollutant inside the shallow bay. Fig. 14 shows the concentration decay curves for 9 bays of the same width at $W/B = 0.25$ and it is obvious that the decay is much slower for the deeper bays. Another observation is that the heights of the bays do not significantly affect the decay curves.

Fig. 15 compares the retention times of the 27 re-entrant bays on the building side faces. It is worth noting that the range of retention times is a few times those for the windward and leeward bays in Fig. 12. As contrast to the windward or leeward bays, the retention time does not depend on the building or bay height, except for the deepest bays at $D/B = 0.375$ where a taller height leads to slightly longer retention time. This is because the dispersion of pollutant mostly occurs evenly along the building height (Fig. 13). Obviously, the retention time is strongest affected by the bay depth. This is indeed observed in the figure where the nine curves are separated into three groups with the deepest bays at $D/B = 0.375$ occupying the three uppermost curves of the longest retention times and the

shallowest bays at D/B = 0.125 making the three lowermost curves of the shortest retention times. The width of the bay also affects the retention time with a shorter retention time for a wider bay but the effect is not as strong as the bay depth. It can also be stated that the ventilation efficiency of the side bays depends on their cross-sectional areas ($W \times D$).

6. Conclusions

This paper presented a systematic CFD study of wind-induced natural ventilation and pollutant transport of re-entrant bays on a high-rise building. A total of 30 generic building models of different building heights; 27 of them installed with re-entrant bays of different dimensions, are investigated. All buildings have an "**H**"-sectional shape of the square envelope and two re-entrant bays are installed on two opposite faces of the building along the full building height. The parameters being varied include the bay width having dimensions W/B = {0.25, 0.50, 0.75}, bay depth having dimensions D/B = {0.125, 0.25, 0.375}, and building height at H/B = {4, 6, 8}. Computation of the mean wind flow around each building model and inside the bays is carried out by RANS and with standard k-ε model for turbulence closure. Natural wind profiles of the open land exposure are used as the inlet boundary conditions. After solution of the mean flow field, the entire re-entrant bay is filled with a scalar species at uniform concentration and subsequent dispersion of the scalar by wind-induced ventilation of the bay is computed using the mean flow field.

The results revealed that the external wind flow around a building is not significantly altered by the presence of a re-entrant bay. Whether a re-entrant bay is on the

windward, leeward or side face of the building, the induced flow inside it occurs at slow velocities. The flow inside a bay on the side face of the building is highly 3D and very complex while the flow inside a windward or leeward bay is simpler. For a re-entrant bay on the windward face of the building, flow stagnation point occurs in the time-averaged sense at $z/H \approx 0.8$ and flow entering the bay above this height escapes through the roof opening. On lower heights, flow mainly travels downwards inside the bay and escapes upwind near the ground level. Of the bays on different faces of a building, the windward bays are the best ventilated with the shortest retention times. The retention time increases with the height of the building and the ventilation improves with a wider and narrower bay. The flow pattern inside a bay on the leeward side of the building is very much the reverse of that of the windward bay. Air is sucked into the bay from the building wake at an upper height and escapes through the roof opening and near the ground level. The flow rate is less than the windward bay and the retention time is about 1.5 longer.

A re-entrant bay on the side face of the building is not actively ventilated. The air exchange rate with the external wind flow is much slower than that of the windward or leeward bay. The retention time of the trapped pollutant is a few times longer. The flow is highly 3D and complicated. On the horizontal plane, a recirculation vortex is observed inside the bay and the vortex is particularly well developed for bays having W/D near unity. On the vertical plane, two secondary-flow vortical structures with streamwise vorticity are observed. One vortex is located near the ground bringing air from outside into the bay at levels near the ground and ejecting air at $z/H \approx 0.2$ to 0.4. Another vortex is located below the roof opening. Between the two vortices, flow inside the bay is mainly downward over a large and middle portion of the bay height. Air exchange between the bay and outside

occurs over most of the bay height. As a result, the ventilation efficiency of the side re-entrant bay, as measured by the retention time of pollutant, does not depend significantly on the building height. The determining factor is the bay depth followed by the bay width.

This study does not consider buoyant pollutant and heat discharge. In those cases, buoyancy acts as an additional factor for flow and scalar transport inside the bays. As an implication to the ventilation design of the re-entrant bays, our results show that the depth of the bay reduces the ventilation efficiency in a significant manner. The bays on the building side face are much worse ventilated than the windward or leeward bays but their ventilation efficiency is not affected by the building height which plays a governing effect on the pollutant dispersion for the later two types of re-entrant bays. In general, air exchange and pollutant dispersion are the worst in taller and deeper bays. In these conditions, wind-induced flow by the natural wind might not be able to take away harmful gaseous discharges or waste heat from the bays. In the worst case, disastrous events like the Amoy Garden Crises would result. Therefore, it will be suggested that to deploy a shallow recessed re-entrant bay, say depth not larger than 1/8 the building breadth.

Acknowledgements

This investigation is supported by a grant awarded by the Research Grants Council of Hong Kong (HKU/713507). The CFD resource is partially supported by the centre of Applied Computing and Interactive Media, City University of Hong Kong.

References

Aldawoud, A., Clark, R., 2008. Comparative analysis of energy performance between courtyard and atrium in buildings, Energy and Buildings 40(3), 209–214.

Ansys CFX-solver theory guide, 2009. Turbulence and wall function, Chapter 2, 53-54.

Cheng, C.K., Yuen, K.K., Lam, K.M., Lo, S.M., 2005. CFD wind tunnel test: Field velocity patterns of wind on a building with a refuge floor, International Journal of Computational Fluid Dynamics 19(7), 531-544.

Cheng, C.K., Lam, K.M., Yuen, K.K., Lo, S.M., Liang, J., 2007. A study of natural ventilation in a refuge floor, Building and Environment 42(9), 3322-3332.

Cheng, C.K., Lam, K.M., Demirbilek, F.N., 2008. Effects of building wall arrangements on wind-induced ventilation through the refuge floor of a tall building, Journal of Wind Engineering and Industrial Aerodynamics 96(5), 656-664.

Cheng, C.K., 2009. A fire safety of Hong Kong refuge floor building wall layout design, Fire Safety Journal 44(4), 545-558.

Chow, T.T., Lin, Z., Liu, J.P., 2002. Effect of condensing unit operation on kitchen exhaust at residential tower, Journal of Architectural Science Review 45, 3-12.

Cook, N.J., 1985. The designer's guide to wind loading of building structure, Part II: Static structures, Building Research Establishment, Watford, 1985.

Gomes, M.G., Rodrigues, A.M., Mendes, P., 2005. Experimental and numerical study of wind pressures on irregular-plan shapes, Journal of Wind Engineering and Industrial Aerodynamics 93(10), 741-756.

Higson, H.L., Griffiths, R.F., Jones, C.D., Hall, D.J., 1996. Flow and dispersion around an isolated building, Atmospheric Environment, 30(16), 2859-2870.

Hong Kong Government, 2004. Outbreak at the Amoy Garden, In: Report of the Select Committee to inquire into the handling of the Severe Acute Respiratory Syndrome outbreak by the Government and the Hospital Authority, http://www.legco.gov.hk/yr03-04/english/sc/sc_sars/report/ch8.pdf

Kijewski, T., Kareem, A., 1998. Dynamic wind effects: a comparative study of provisions in codes and standards with wind tunnel data, Wind and Structures 1(1), 77-109.

Lam, K.M., To, A.P., 2006. Reliability of numerical computation of pedestrian level wind environment around a row of tall buildings, Wind and Structures 9(6), 473-492.

Lam, K.M., Leung, M.Y.H. and Zhao, J.G., 2008. Interference effects on wind loading of a row of closely spaced tall buildings, Journal of Wind Engineering and Industrial Aerodynamics 96(5), 562-583.

Launder, B.E., Spalding, D.B., 1974. The numerical computation of turbulent flows, Computer Methods In Applied Mechanics and Engineering 3, 269-289.

Rajapaksha, I., Nagai, H., Okumiya, M., 2003. A ventilated courtyard as a passive cooling strategy in the warm humid tropics, Renewable Energy 28(11), 1755–1778.

Santos, J.M., Griffiths, R.F., Robert, I.D., Reis Jr, N.C., 2005. A field experiment on turbulent concentration fluctuations of an atmospheric tracer gas in the vicinity of a complex-shaped building, Atmospheric Environment 39(28), 4999-5012.

Sharples, S., Bensalem, R., 2001. Airflow in courtyard and atrium buildings in the urban environment: A wind tunnel study, Solar Energy 70(3), 237-244.

Tominaga, Y., Mochida, A., Yoshie, R., Kataoka, H., Nozu, Tsuyoshi, Yoshikawa, M., 2008, AIJ guidelines for practical applications of CFD to pedestrian wind environment around buildings, Journal of Wind Engineering and Industrial Aerodynamics 96(10-11), 1749-1761.

Yeoh, E.K., 2003. Severe acute respiratory syndrome: Response from Hong Kong, Hong Kong Government,

http://www.who.int/csr/sars/conference/june_2003/materials/presentations/en/sarshksar17063.pdf

Yim, S.H.L., Fung, J.C.H., Lau, A.K.H., Kot, S.C., 2009. Air ventilation impacts of the "wall effect" resulting from the alignment of high-rise buildings, Atmospheric Environment 43(32), 4982-2894.

Yu, T.S., Li Y.G., Wong, T.W., Tam, W., Chan, A.T., Lee, J.H.W., Leung, D.Y.C., Ho, T., 2004. Evidence of airborne transmission of the severe acute respiratory syndrome virus, New England Journal of Medicine 350(17), 731-1739.

Zhou, Y., Kijewski, T., Kareem, A., 2003. Aerodynamic loadings: Interactive Database, Journal of Structural Engineering, ASCE March 2003, 394-404.

Figure Captions

Fig. 1. Computational mesh for a 4*B* tall building model: (a) 3D computational domain; (b) central vertical plane.

Fig. 2. Comparison of computed and wind tunnel data obtained in the previous wind flow study of a refuge floor design (Cheng *et al*. 2005).

Fig. 3. Mean velocity vectors from wind tunnel measurement and CFD simulation results at the building horizontal symmetry plane of a 6*B* tall building with Case 2 re-entrant bay on building side faces (wind angle 90^o).

Fig. 4. Mean wind velocity vectors patterns on the major building flow planes: (a) 6*B* tall square planned building at wind angle 0^o; (b) 6*B* tall building with Case 2 re-entrants bay at wind angle 0^o; (c) 6*B* tall building with Case 2 re-entrant bays at wind angle 90^o.

Fig. 5. Mean wind velocity vectors patterns and C_p contour on the major symmetry flow planes of the 6*B* tall building with Case 9 re-entrant bays at wind angle 0^o: (a) Horizontal plane at mid-height; (b) central vertical plane (vertical scale compressed).

Fig. 6. Velocity coefficients for windward and leeward re-entrant bays at wind angle 0^o: (a) $C_n(z)$ for windward bays; (b) $C_n(z)$ for leeward bays; (c) $C_w(H)$ through building roofs.

Fig. 7. Mean wind velocity vectors patterns and C_p contour on the major $8B$ tall building with Case 9 re-entrant bay at wind angle 90^o: (a) Horizontal plane at mid-height; (b) central vertical plane (vertical scale compressed).

Fig. 8. Vertical velocity coefficients at wind angle 90^o: (a) $C_w(H)$ through building roofs; (b) $C_w(z)$ along height of side re-entrant bay.

Fig. 9. Normal velocity coefficient $C_n(z)$ along height of side bay at wind angle 90^o.

Fig. 10. Pollutant dispersion (C/C_o) sequences from the re-entrant bay installing at $8B$ tall building (vertical scale compressed) with Case 3 re-entrant bay at wind angle 0^o (only symmetry vertical plane is shown): (a) Windward side bay; (b) leeward side bay.

Fig. 11. Concentration-time decay curves of windward re-entrant bays of $W/B = 0.25$ at wind angle 0^o.

Fig. 12. Retention time of re-entrant bays on 27 building models at wind angle 0^o: (a) Windward bays; (b) leeward bays.

Fig. 13. Pollutant dispersion (C/C_o) from re-entrant bay on side face of 8B tall building (vertical scale compressed) at wind angle 90^o (Only symmetry vertical plan is shown): (a) Deep bay (W/B = 0.25; D/B = 0.375); (b) narrow bay (W/B = 0.25; D/B = 0.125).

Fig. 14. Concentration-time decay curves of re-entrant bays of W/B = 0.25 on side faces of buildings at wind angle 90^o.

Fig. 15. Retention time of re-entrant bays on side faces of 27 building models at wind angle 90^o.

Table 1: Building configurations: dimensions and aspect ratio of re-entrant bays.

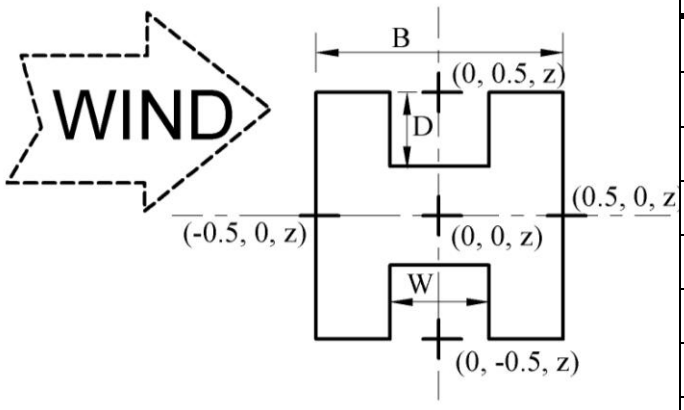

Case No.	Width (W/B)	Depth (D/B)
1	0.25	0.125
2	0.25	0.250
3	0.25	0.375
4	0.50	0.125
5	0.50	0.250
6	0.50	0.375
7	0.75	0.125
8	0.75	0.250
9	0.75	0.375

Figure(s)

(a)

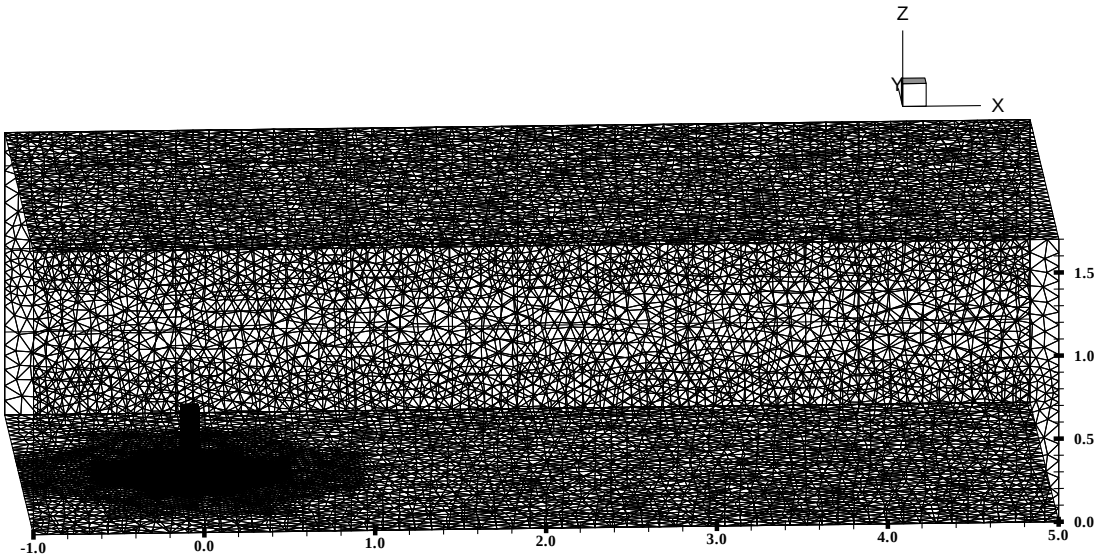

(b)

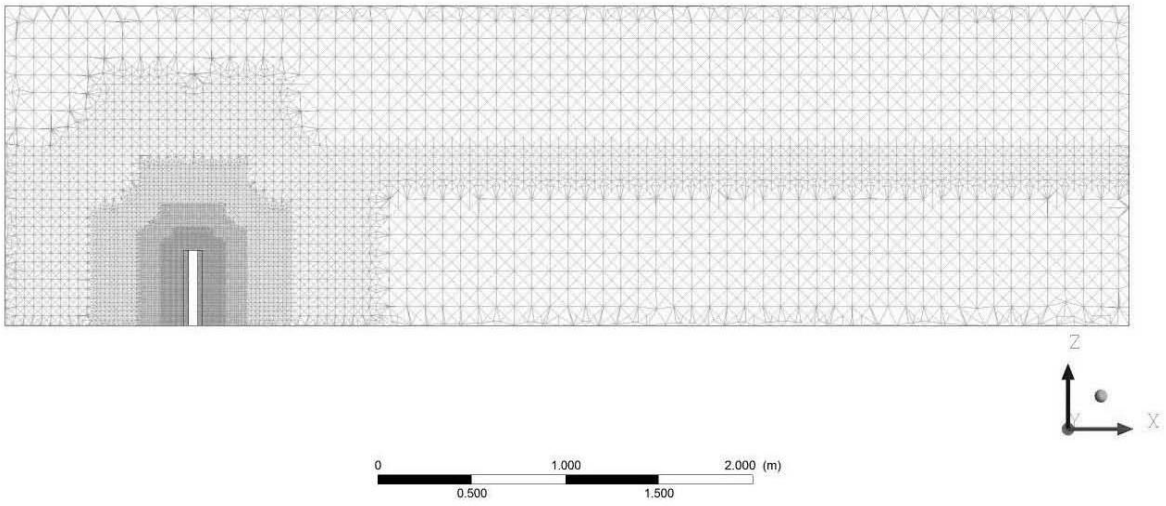

Fig. 1. Computational mesh for a 4*B* tall building model: (a) 3D computational domain; (b) central vertical plane.

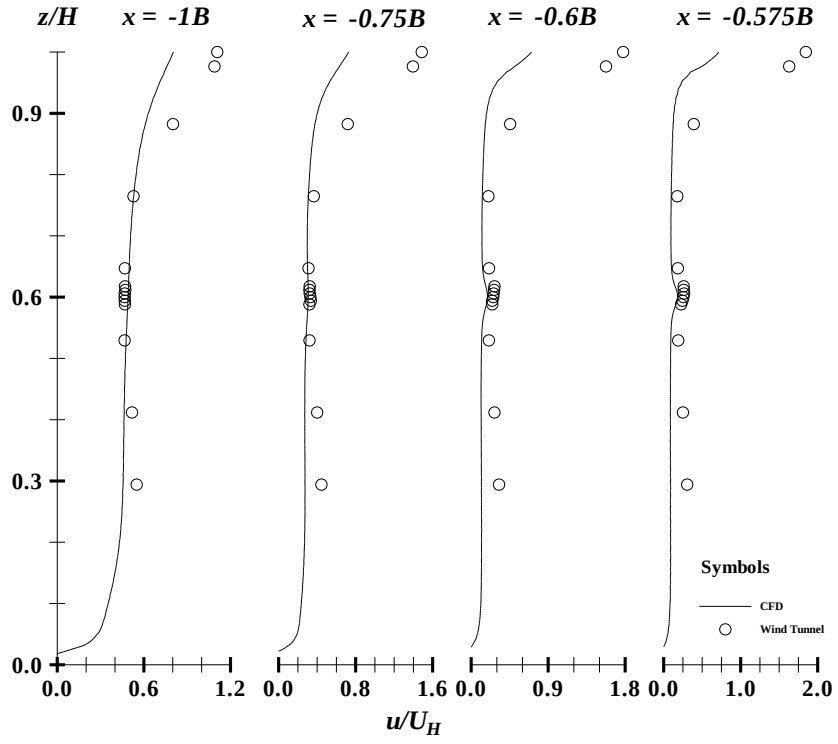

Fig. 2. Comparison of computed and wind tunnel data obtained in the previous wind flow study of a refuge floor design (Cheng *et al*. 2005).

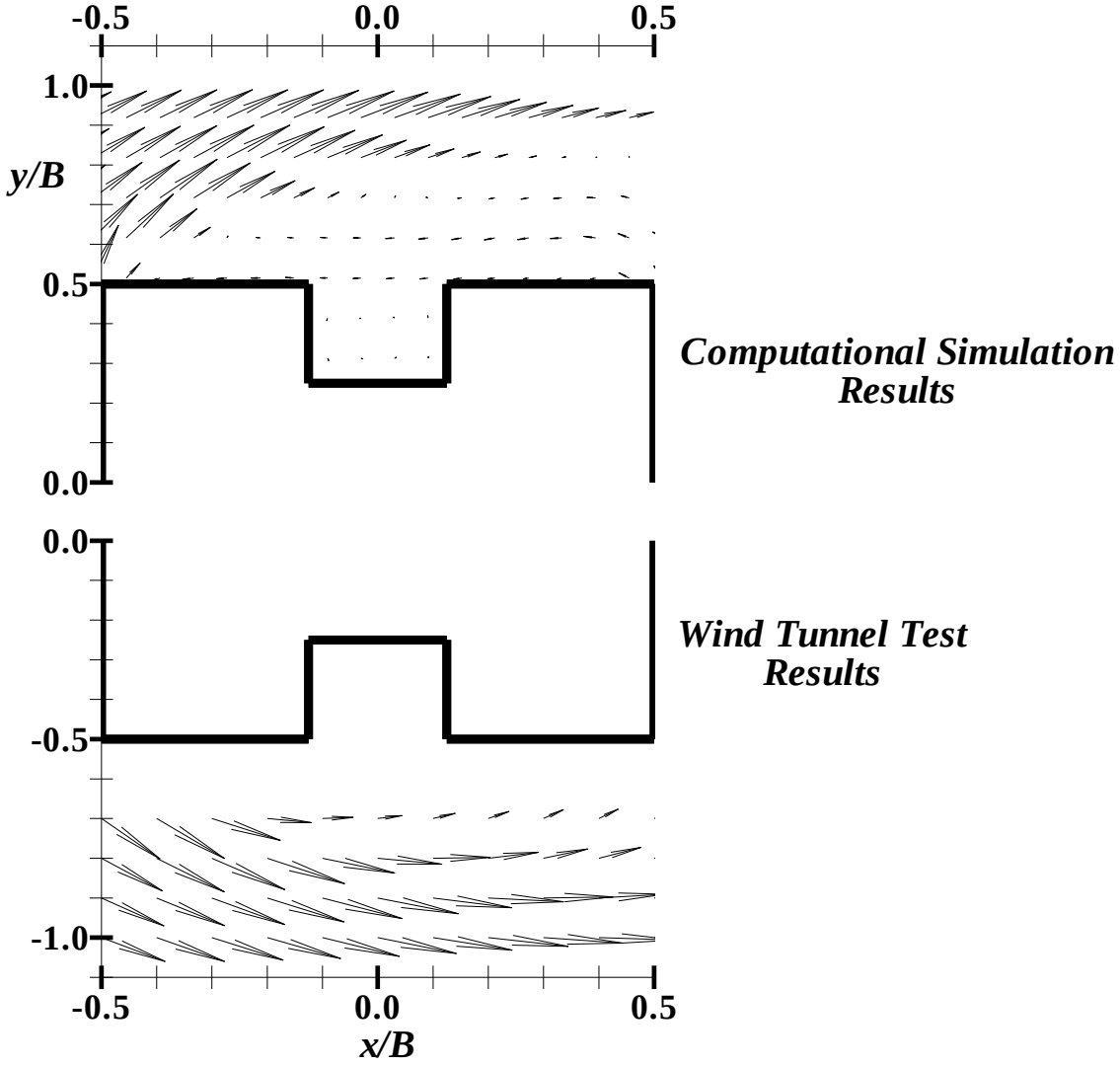

Fig. 3. Mean velocity vectors from wind tunnel measurement and CFD simulation results at the building horizontal symmetry plane of a 6*B* tall building with Case 2 re-entrant bay on building side faces (wind angle 90^{o}).

28 (a)

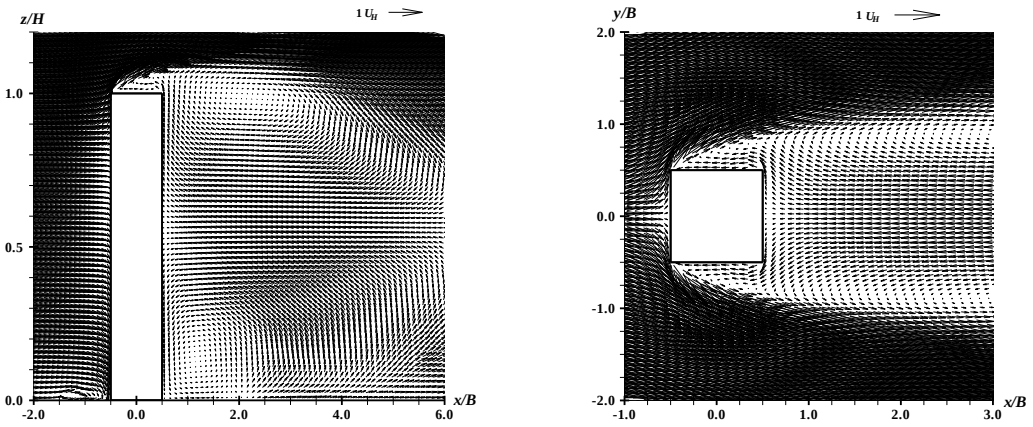

29 (b)

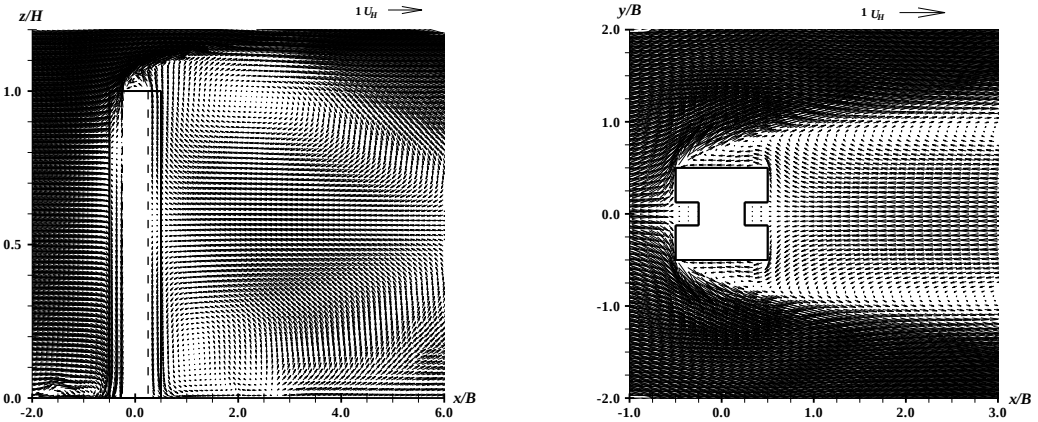

30 (c)

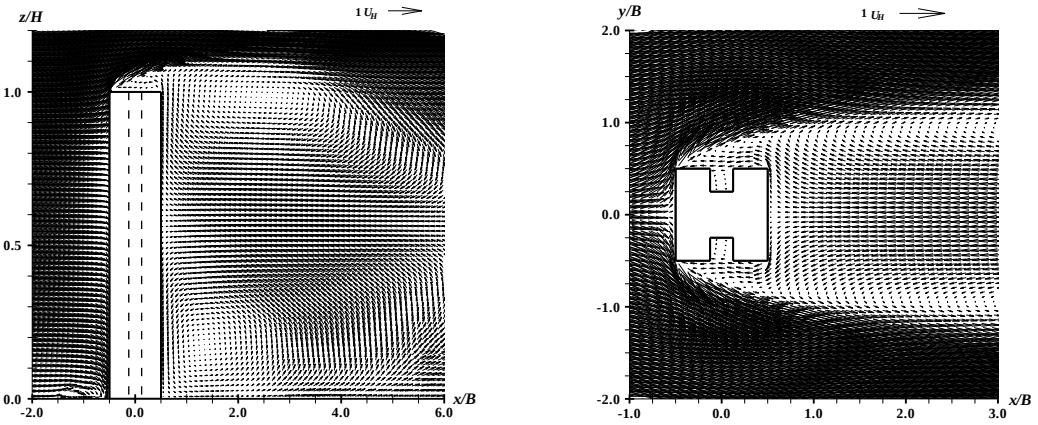

31 Fig. 4. Mean wind velocity vectors patterns on the major building flow planes: (a) 6*B* tall
32 square planned building at wind angle 0^o; (b) 6*B* tall building with Case 2 re-entrants bay at
33 wind angle 0^o; (c) 6*B* tall building with Case 2 re-entrant bays at wind angle 90^o.

(a)

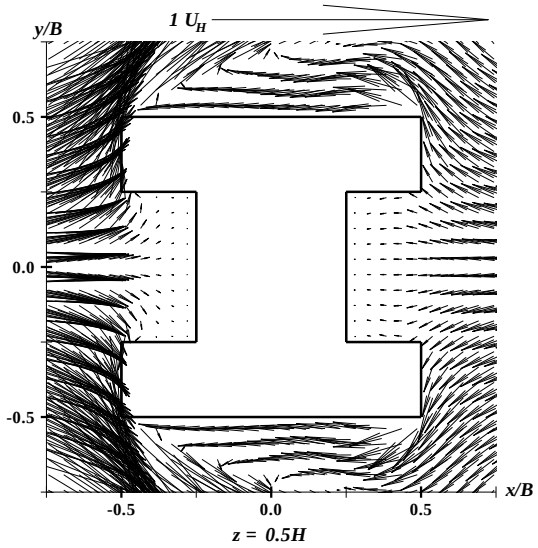

(b)

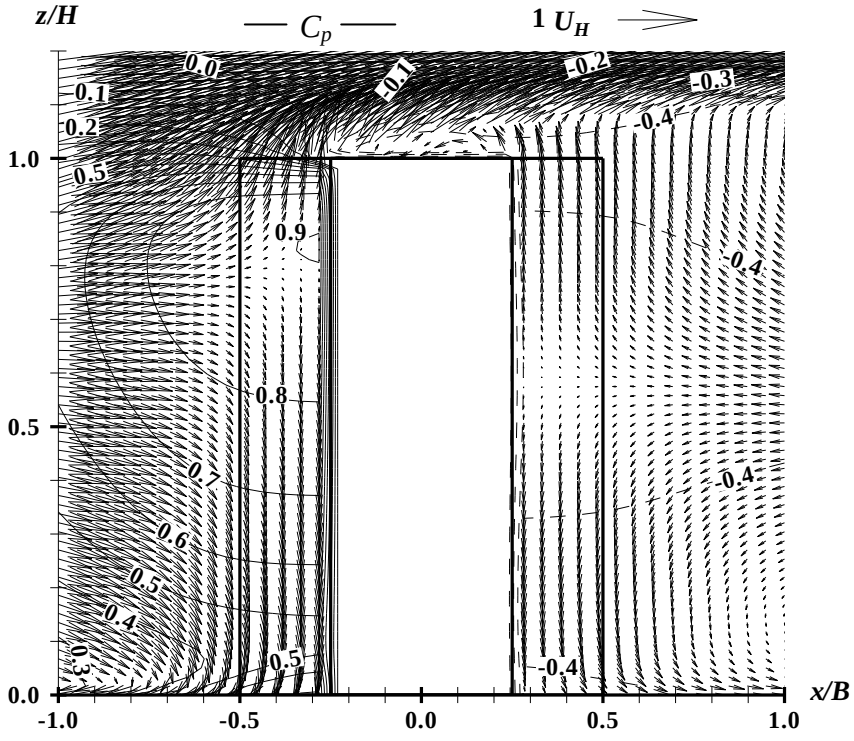

Fig. 5. Mean wind velocity vectors patterns and C_p contour on the major symmetry flow planes of the 6*B* tall building with Case 9 re-entrant bays at wind angle 0^o: (a) Horizontal plane at mid-height; (b) central vertical plane (vertical scale compressed).

(a)

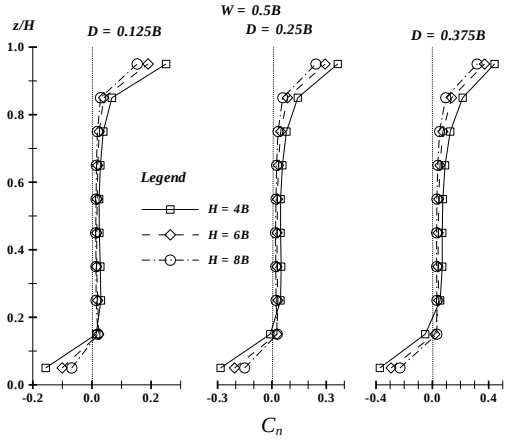

(b)

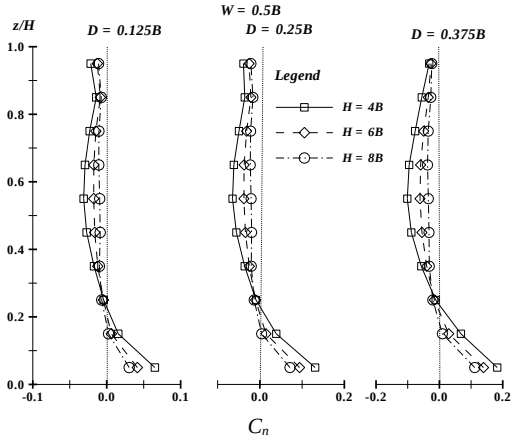

(c)

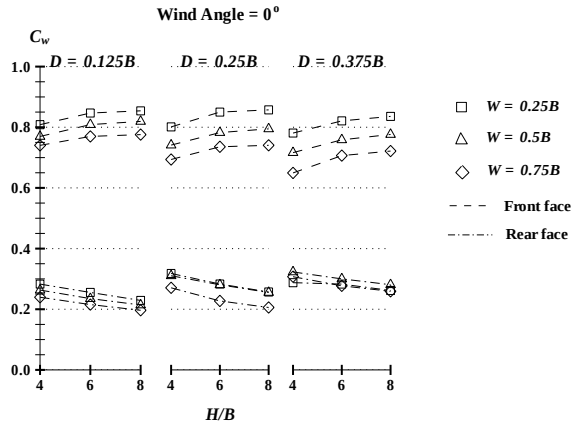

Fig. 6. Velocity coefficients for windward and leeward re-entrant bays at wind angle 0^o: (a) $C_n(z)$ for windward bays; (b) $C_n(z)$ for leeward bays; (c) $C_w(H)$ through building roofs.

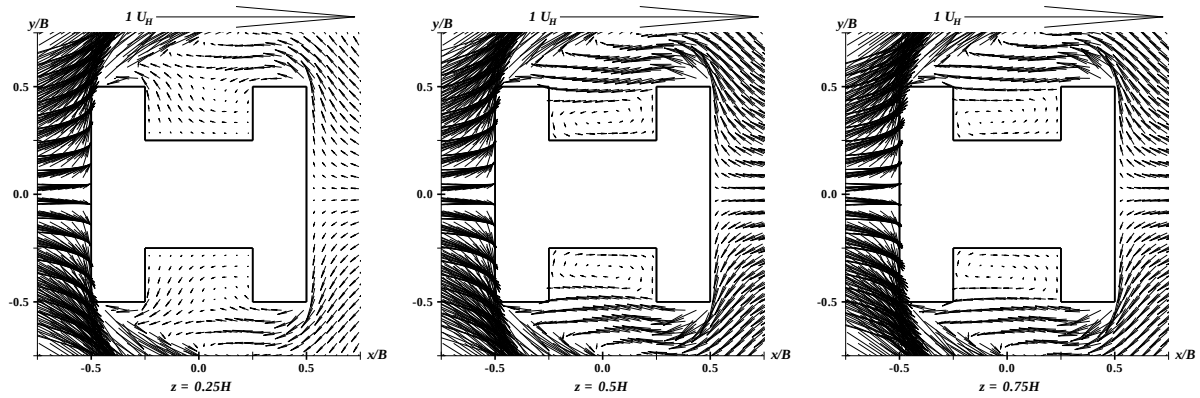

(a)

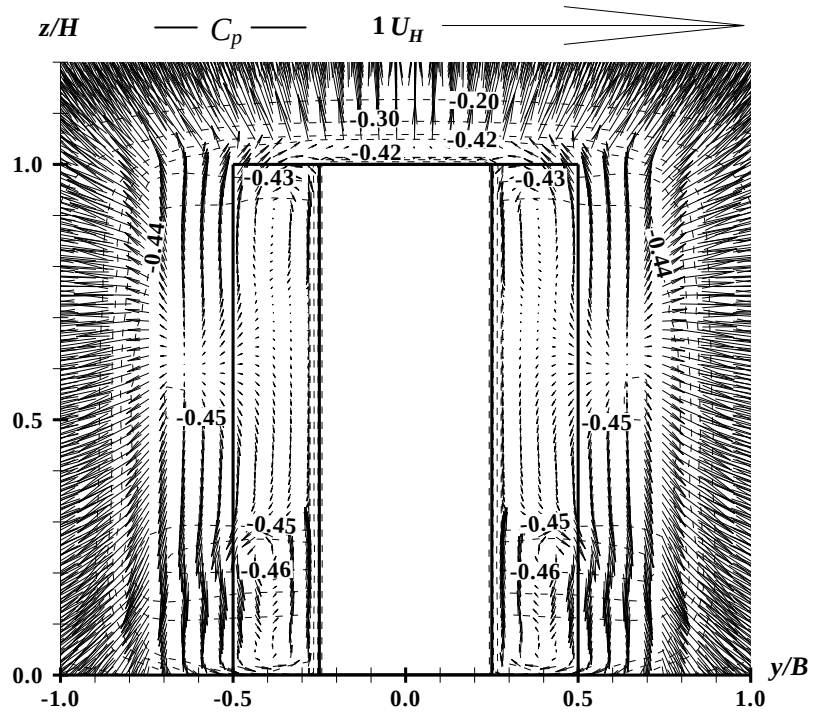

(b)

Fig. 7. Mean wind velocity vectors patterns and C_p contour on the major 8*B* tall building with Case 9 re-entrant bay at wind angle 90^o: (a) Horizontal plane at mid-height; (b) central vertical plane (vertical scale compressed).

64 (a)

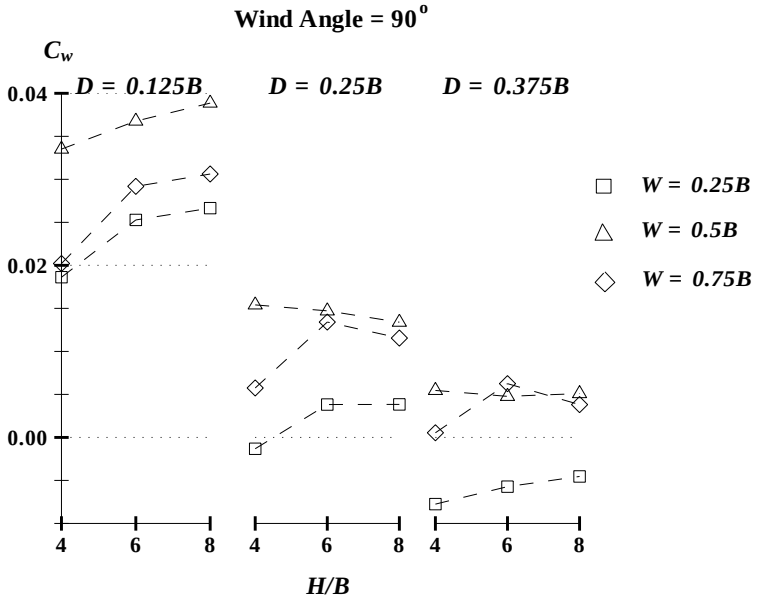

65

66 (b)

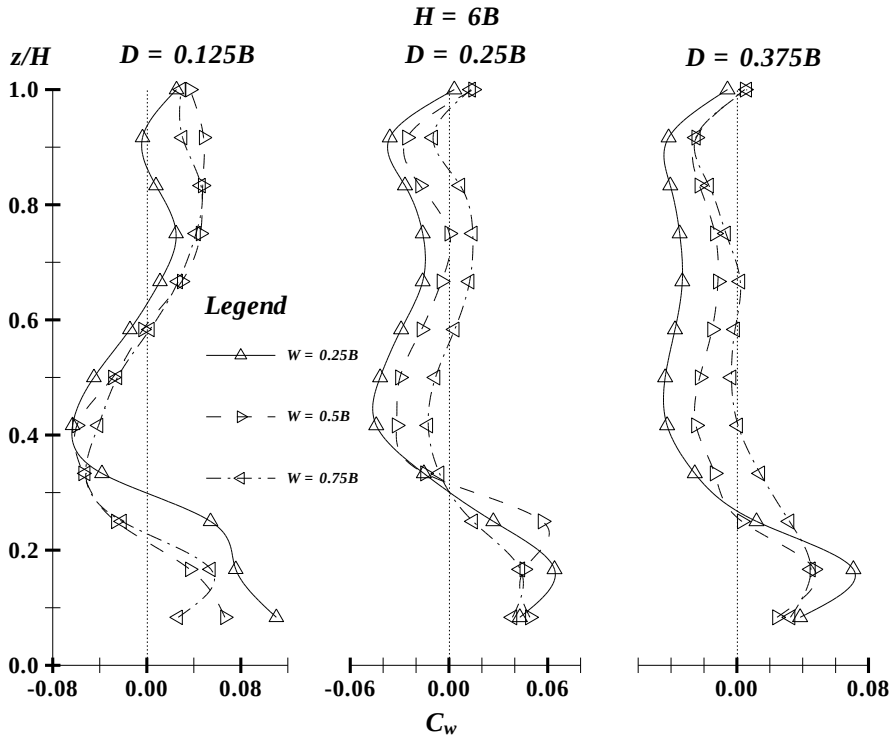

67

68 Fig. 8. Vertical velocity coefficients at wind angle 90°: (a) $C_w(H)$ through building roofs;

69 (b) $C_w(z)$ along height of side re-entrant bay.

70

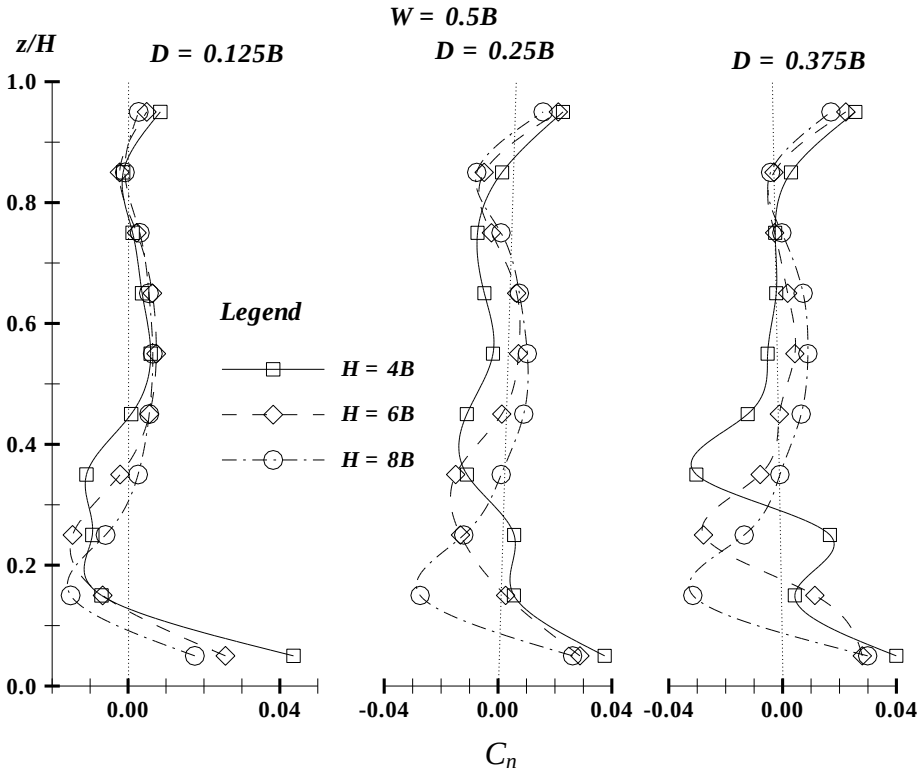

Fig. 9. Normal velocity coefficient $C_n(z)$ along height of side bay at wind angle 90^o.

(a)

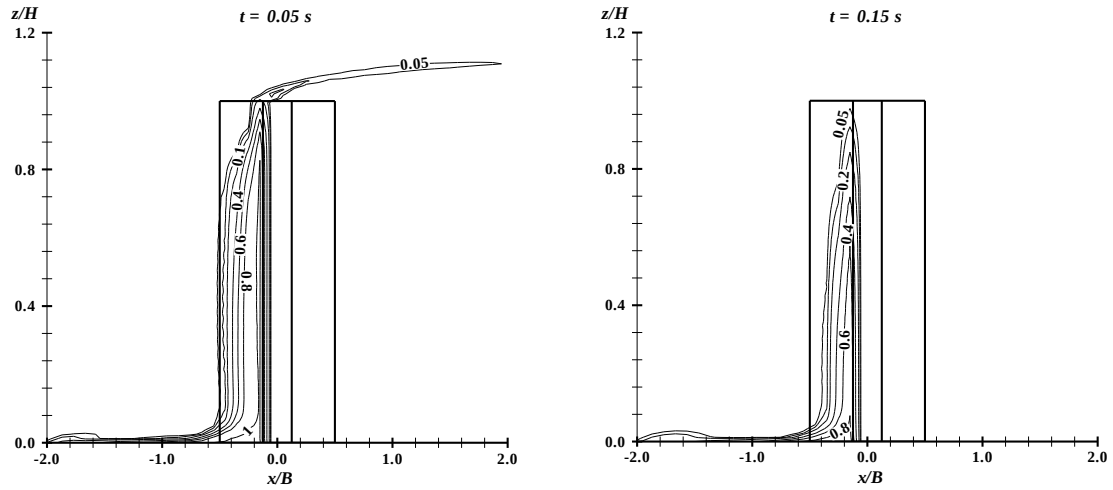

(b)

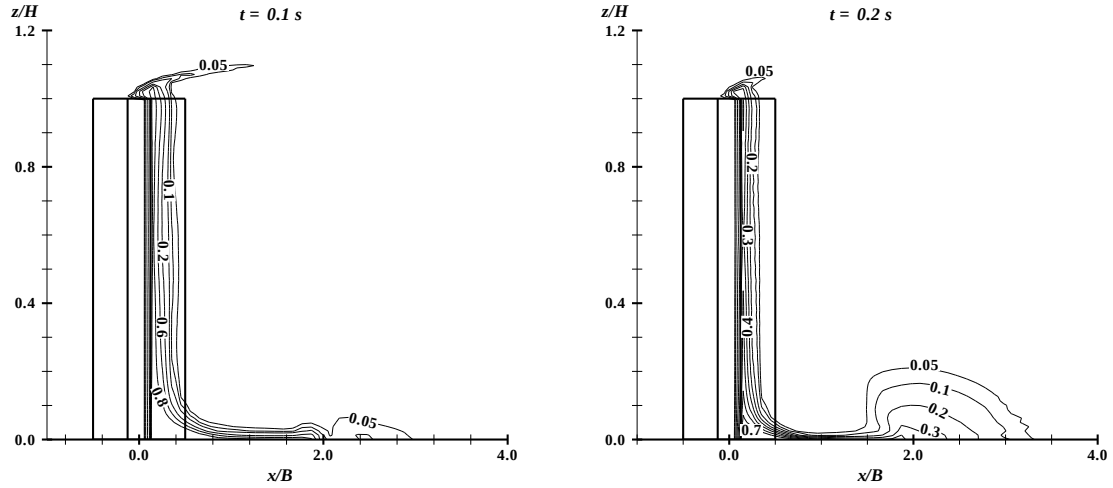

Fig. 10. Pollutant dispersion (C/C_o) sequences from the re-entrant bay installing at 8*B* tall building (vertical scale compressed) with Case 3 re-entrant bay at wind angle 0^o (only symmetry vertical plane is shown): (a) Windward side bay; (b) leeward side bay.

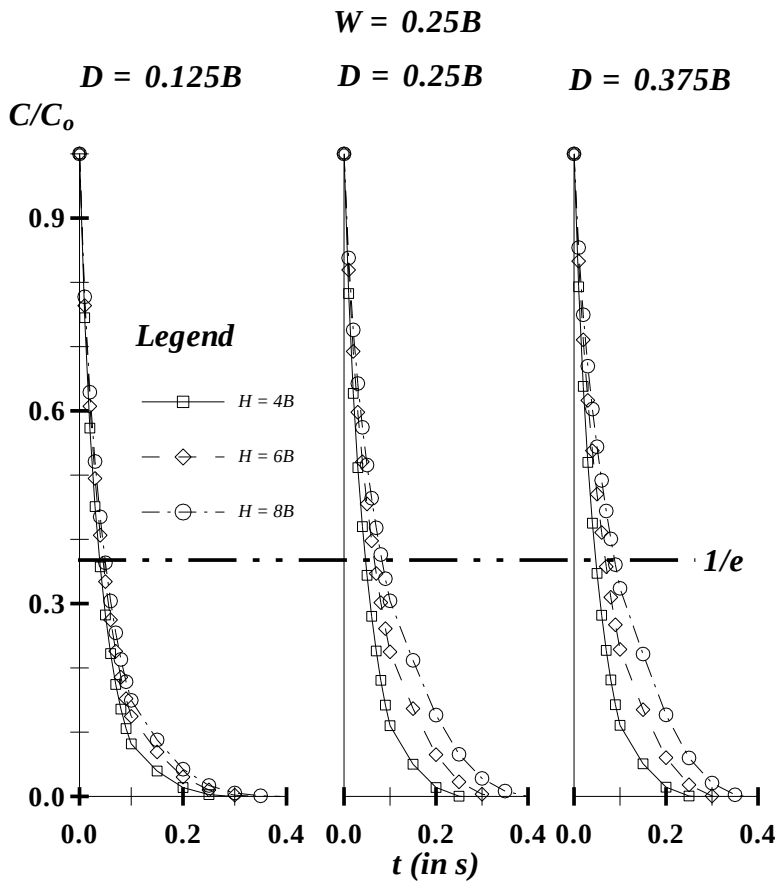

Fig. 11. Concentration-time decay curves of windward re-entrant bays of $W/B = 0.25$ at wind angle 0^o.

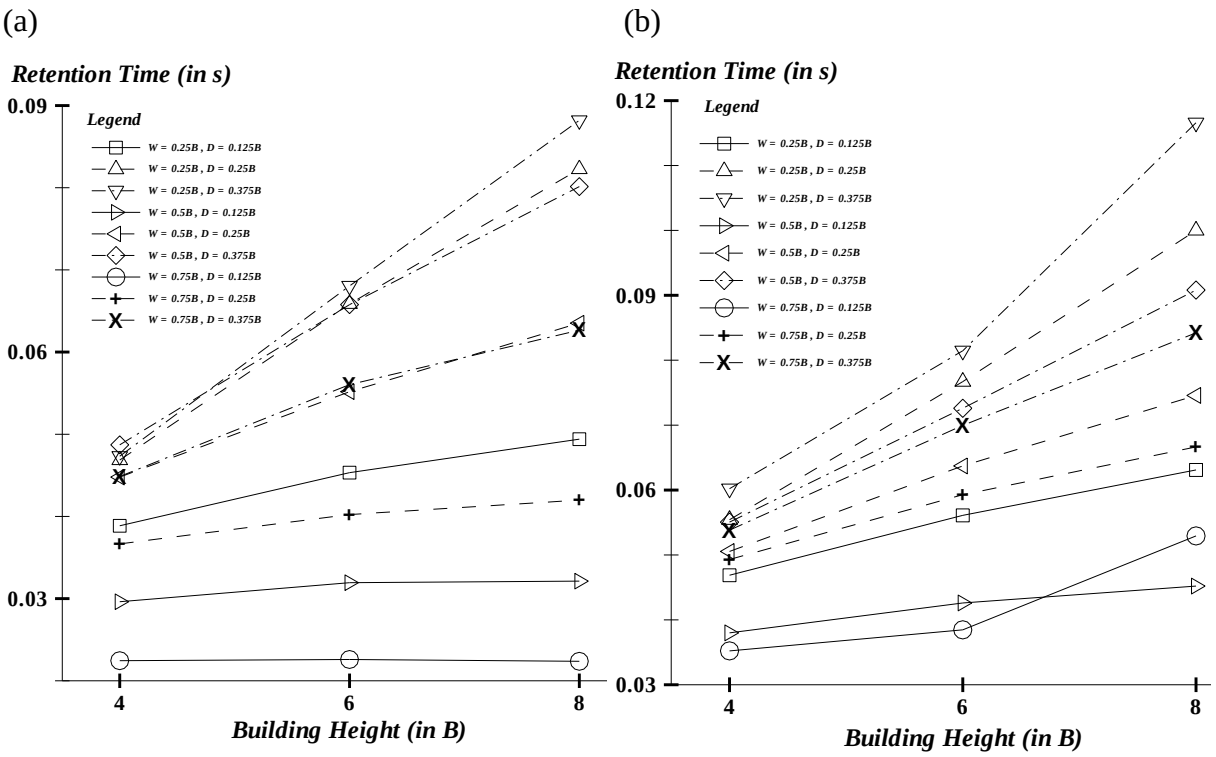

Fig. 12. Retention time of re-entrant bays on 27 building models at wind angle 0^{o}: (a) Windward bays; (b) leeward bays.

(a)

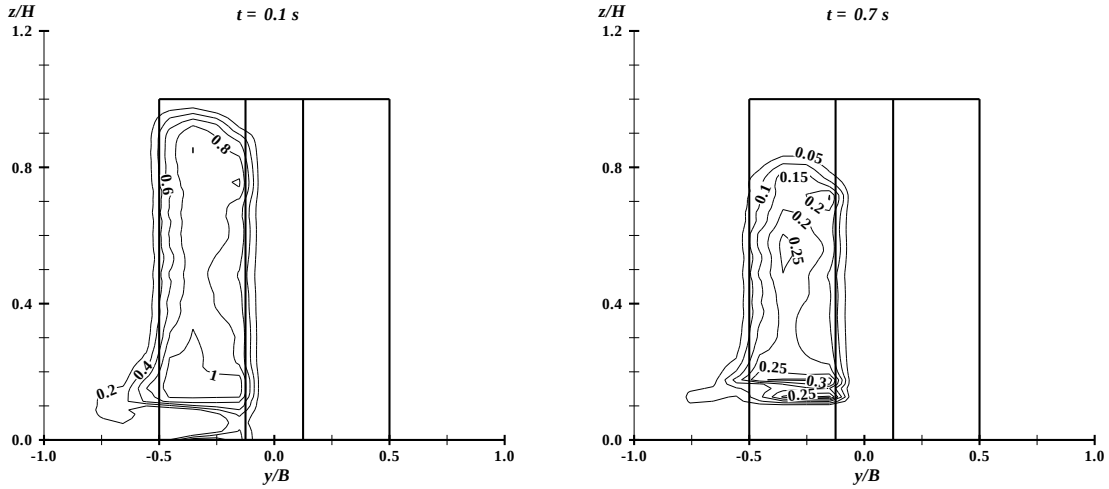

(b)

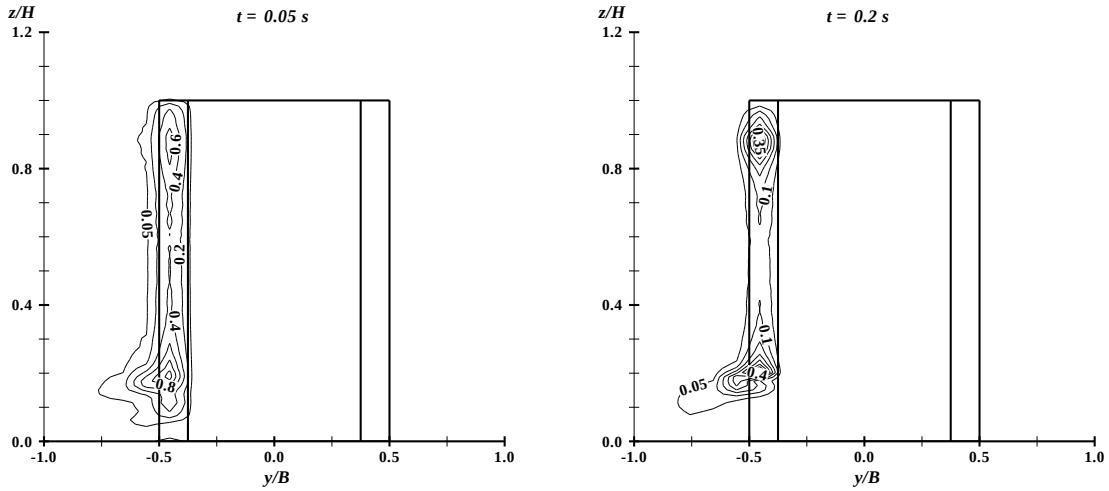

Fig. 13. Pollutant dispersion (C/C_o) from re-entrant bay on side face of 8B tall building (vertical scale compressed) at wind angle 90^o (Only symmetry vertical plan is shown): (a) Deep bay (W/B = 0.25; D/B = 0.375); (b) narrow bay (W/B = 0.25; D/B = 0.125).

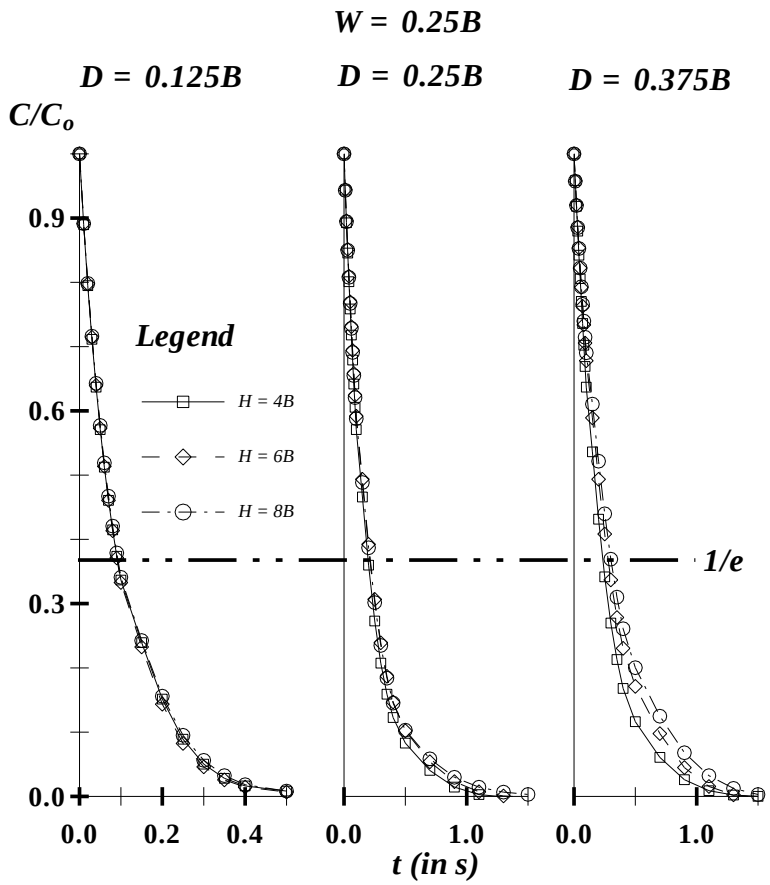

Fig. 14. Concentration-time decay curves of re-entrant bays of W/B = 0.25 on side faces of buildings at wind angle 90^{o}.

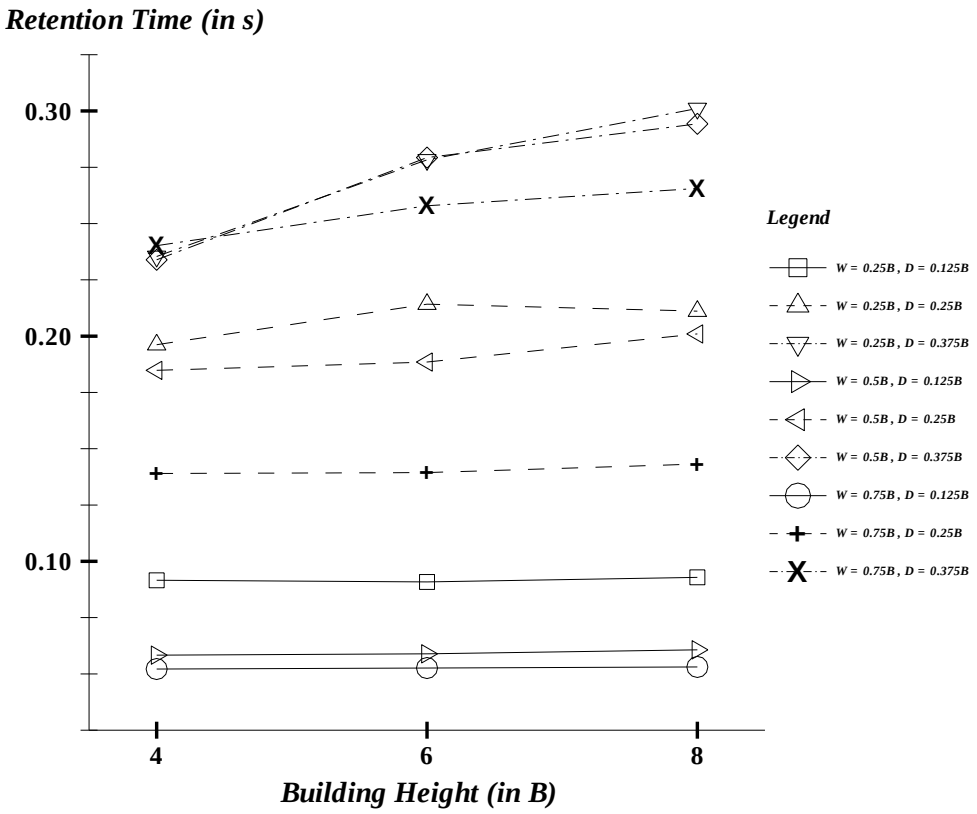

Fig. 15. Retention time of re-entrant bays on side faces of 27 building models at wind angle 90^{o}.